

Article

Facile Synthesis of Nano-Flower β - $\text{Bi}_2\text{O}_3/\text{TiO}_2$ Heterojunction as Photocatalyst for Degradation RhB

Mingjun Wang ^{1,2,†}, Che Li ^{2,†}, Bingfang Liu ^{1,2}, Wenzhen Qin ^{2,*} and Yu Xie ^{2,*} ¹ Academy of Art & Design, Nanchang Institute of Technology, Nanchang 330044, China² College of Environment and Chemical Engineering, Nanchang Hangkong University, Nanchang 330063, China

* Correspondence: qwz1417@163.com (W.Q.); xieyu_121@163.com (Y.X.)

† These authors contributed equally to this work.

Abstract: Photocatalysis is a hopeful technology to solve various environmental problems, but it is still a technical task to produce large-scale photocatalysts in a simple and sustainable way. Here, nano-flower β - $\text{Bi}_2\text{O}_3/\text{TiO}_2$ composites were prepared via a facile solvothermal method, and the photocatalytic performances of β - $\text{Bi}_2\text{O}_3/\text{TiO}_2$ composites with different Bi/Ti molar ratios were studied. The nano-flower $\text{Bi}_2\text{O}_3/\text{TiO}_2$ composites were studied by SEM, XRD, XPS, BET, and PL. The PL result proved that the construction of staggered heterojunction enhanced the separation efficiency of carriers. The degradation RhB was applied to study the photocatalytic performances of prepared materials. The results showed that the degradation efficiency of RhB increased from 61.2% to 99.6% when the molar ratio of Bi/Ti was 2.1%. It is a mesoporous approach to enhance photocatalytic properties by forming heterojunction in $\text{Bi}_2\text{O}_3/\text{TiO}_2$ composites, which increases the separation efficiency of the generated carriers and improves photocatalytic properties. The photoactivity of the $\text{Bi}_2\text{O}_3/\text{TiO}_2$ has no evident changes after the fifth recovery, indicating that the $\text{Bi}_2\text{O}_3/\text{TiO}_2$ composite has distinguished stability.

Keywords: $\text{Bi}_2\text{O}_3/\text{TiO}_2$; heterojunction; photocatalysts; degradation RhB

Citation: Wang, M.; Li, C.; Liu, B.; Qin, W.; Xie, Y. Facile Synthesis of Nano-Flower β - $\text{Bi}_2\text{O}_3/\text{TiO}_2$ Heterojunction as Photocatalyst for Degradation RhB. *Molecules* **2023**, *28*, 882. <https://doi.org/10.3390/molecules28020882>

Academic Editors: Surjyakanta Rana and Orhan Şişman

Received: 20 December 2022

Revised: 5 January 2023

Accepted: 5 January 2023

Published: 16 January 2023



Copyright: © 2023 by the authors. Licensee MDPI, Basel, Switzerland. This article is an open access article distributed under the terms and conditions of the Creative Commons Attribution (CC BY) license (<https://creativecommons.org/licenses/by/4.0/>).

1. Introduction

Environmental pollution and destruction are becoming a vertical global crisis. Organic dye pollutants are directly discharged into water from dyeing textiles. Most dyes, such as RhB, MB, MR, and EY, are non-biodegradable and carcinogenic, which has brought damage to environment and human health [1]. Therefore, developing an environmental harmony, ecological cleanliness, and safe and energy-saving treatment technology for the problem of environment contamination is the most important immediate challenge that human beings must face [2–4].

Photocatalysis offers a clean, gentle reaction conditions, an easy procedure, and safe technology that can degrade the pollution under solar irradiation [4–7]. Photocatalytic technology plays a significant role in the field of environmental pollution protection [8–10]. Metal oxide semiconductors have garnered great attention in pollution treatment owing to their cheap and easy synthesis [11,12]. As a classic semiconductor, titanium dioxide (TiO_2) is the one most generally cited in photocatalytic technology in virtue of its chemical stability, nontoxicity, low price, and high activity [13]. The photocatalytic reaction system and reaction mechanism of TiO_2 were studied [14,15]. In particular, TiO_2 photocatalysts have been explored broadly in the area of environmental pollution and energy transformation [16–18]. However, the TiO_2 photocatalysts also expose many problems, such as the large band gap (3.2 eV), absorption narrow wavelength range light, easy recombination with photogenerated electrons, and holes, which bring about lower photocatalytic efficiency, limiting its application [19,20]. For this reason, modification of TiO_2 for enhancing its photocatalytic properties is needed and crucial. Many different means have been tried

by researchers to change the surface or comprehensive performances of TiO_2 , for instance, doping metal [21], structural adjustment [22], and heterogeneous structure [23,24], thereby promoting the photocatalytic properties. In these modifications, construction of heterojunctions is a promising strategy to improve the separation efficiency of photogenerated charge carriers. TiO_2 united with narrow bandgap semiconductors that are visible-light-responsive would extend the light absorption range and decrease the combination of photogenerated charge carriers, for example, $\text{TiO}_2/\text{ZnFe}_2\text{O}_4$ [25], CdS/TiO_2 [26], $g\text{-C}_3\text{N}_4/\text{TiO}_2$ [27], and $\text{InVO}_4/\text{TiO}_2$ [28].

Among these visible-light-responsive and narrow band gap semiconductors, bismuth oxide (Bi_2O_3) is an up-and-coming semiconductor to construct heterojunctions with TiO_2 , in which the band gap is lower than that of TiO_2 [29]. When Bi_2O_3 is irradiated with visible light, photogenerated holes of the valence band of Bi_2O_3 have strong oxidation, which is beneficial to degrade the pollutions. In addition, Bi_2O_3 has been under comprehensive study due to its excellent physical and chemical properties, low price, and non-toxicity [30–32]. Bi_2O_3 has α , β , γ , δ , ϵ , and ω phases, i.e., six kinds of polymorphs [33]. In particular, $\beta\text{-Bi}_2\text{O}_3$ possesses high light-absorption performances among the six polymorphs, and the band gap is about 2.3 eV [34]. Therefore, the construction of $\beta\text{-Bi}_2\text{O}_3/\text{TiO}_2$ heterojunction structures can be carried out to increase the light response and photocatalytic performances. However, for the case of $\beta\text{-Bi}_2\text{O}_3/\text{TiO}_2$ photocatalytic composites, the preparation methods are complex, including a two-step procedure, photo-deposition, deposition-reduction, and impregnation method [35,36].

Here, in this paper, the $\beta\text{-Bi}_2\text{O}_3/\text{TiO}_2$ heterojunction photocatalysts were prepared via a simple, one-step solvothermal method. The influences of the molar ratios of $\beta\text{-Bi}_2\text{O}_3/\text{TiO}_2$ on the photocatalytic degradation of RhB for $\beta\text{-Bi}_2\text{O}_3/\text{TiO}_2$ were assessed. In the meantime, the morphology, crystal structure, surface chemical optical state, and photoelectrochemical properties of photocatalysts were investigated.

2. Results and Discussion

2.1. Characterization of Photocatalysts

Figure 1 shows the XRD patterns of pure Bi_2O_3 , pure TiO_2 , and $\text{Bi}_2\text{O}_3/\text{TiO}_2$ photocatalysts with different molar ratios of Bi. For the pure TiO_2 , the diffraction peaks are at 25.3° , 37.8° , 48.1° , 53.9° , and 62.7° , coinciding with (101), (004), (200), (105), and (204) of the anatase TiO_2 (JCPDS No.21-1272) [37]. For pure Bi_2O_3 , the diffraction peaks are corresponding to $\beta\text{-Bi}_2\text{O}_3$ [32]. For $\text{Bi}_2\text{O}_3/\text{TiO}_2$ composites with different molar ratios of Bi, it is evident that the diffraction peaks are similar to pure TiO_2 and correspond to the anatase TiO_2 . The diffraction peak of the Bi phase is not observed in $\text{Bi}_2\text{O}_3/\text{TiO}_2$ composites for several reasons. The size of Bi is extremely small and highly dispersed, and the doping amount of Bi is too small [36]. There are similar results in the reported literatures [38]. For example, Zhu et al. [39] found that $\text{Bi}_2\text{O}_3/\text{TiO}_2$ lacks the Bi_2O_3 diffraction even when the Bi/Ti ratio in $\text{Bi}_2\text{O}_3/\text{TiO}_2$ was 4.1%.

The morphologies of materials were analyzed via SEM and HRTEM, and the images are displayed in Figures 2 and 3. In Figure 2a, the pure Bi_2O_3 reveals a stuffed, coral-like sphere with a diameter between 50–150 nm. The pure TiO_2 exhibits a flower-like structure (Figure 2b). As shown in Figure 2c–f, the $\text{Bi}_2\text{O}_3/\text{TiO}_2$ composites in different molar ratios of Bi display a flower-like structure that is similar to the morphology of pure TiO_2 . It indicates that the incorporation of Bi_2O_3 does not influence the topography of TiO_2 . In addition, the diameter of the flower-like structure of $\text{Bi}_2\text{O}_3/\text{TiO}_2$ composites is between $5\ \mu\text{m}$ – $10\ \mu\text{m}$, and the thickness diameter of the flower-like structure is about 65 nm. Meanwhile, the EDS was applied to investigate the elemental contents of 2.1% $\text{Bi}_2\text{O}_3/\text{TiO}_2$, and the atomic ratio of Bi/Ti is about 2.9%, as displayed in Table 1.

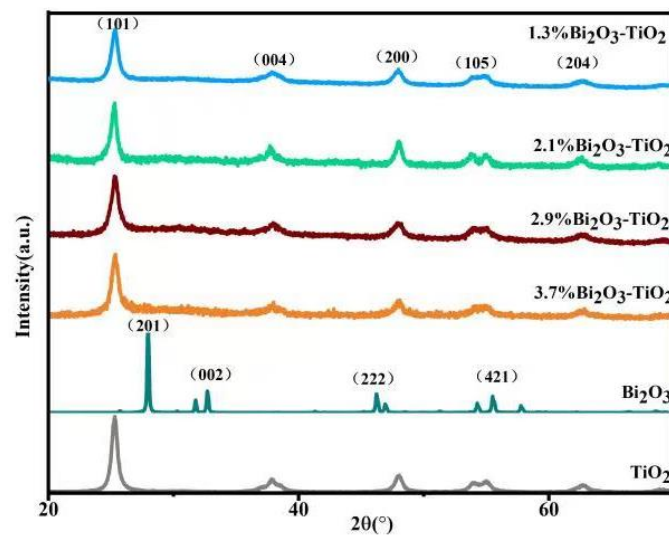


Figure 1. The XRD patterns of β - Bi_2O_3 , TiO_2 , and $\text{Bi}_2\text{O}_3/\text{TiO}_2$ composites.

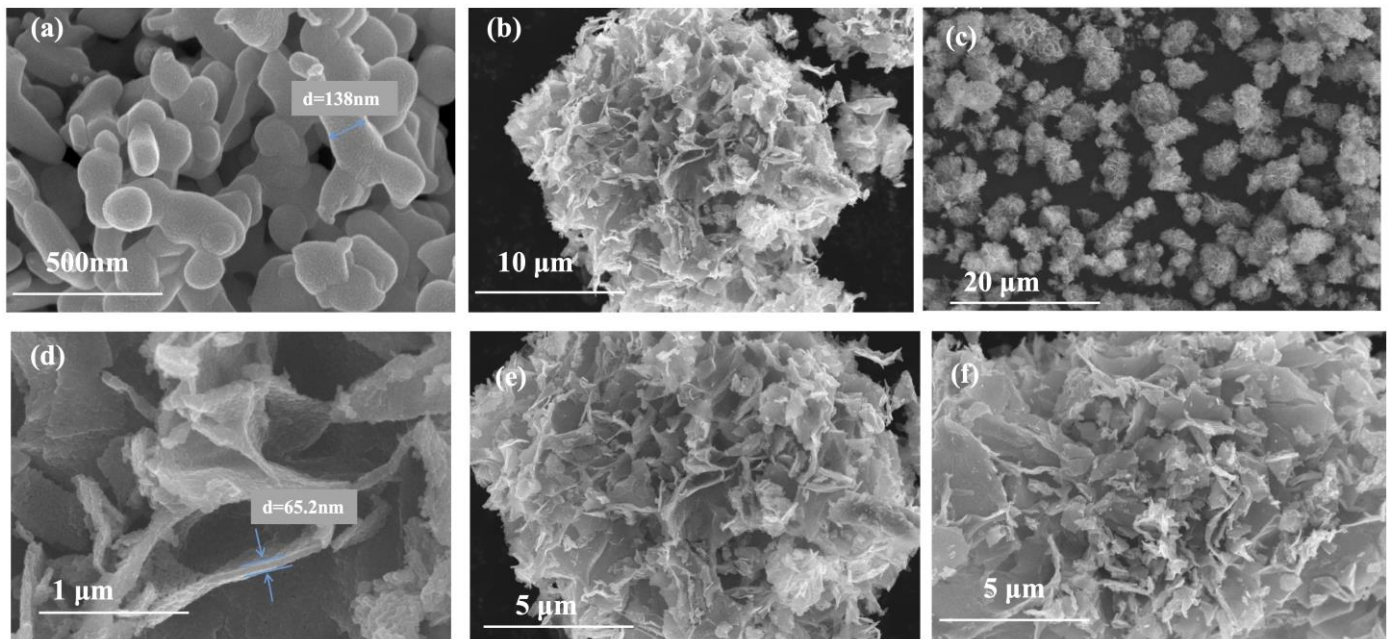


Figure 2. The SEM images of (a) β - Bi_2O_3 , (b) TiO_2 , and (c) 2.1% $\text{Bi}_2\text{O}_3/\text{TiO}_2$; (d) petal diameter of 2.1% $\text{Bi}_2\text{O}_3/\text{TiO}_2$, (e) 2.9% $\text{Bi}_2\text{O}_3/\text{TiO}_2$, and (f) 3.7% $\text{Bi}_2\text{O}_3/\text{TiO}_2$.

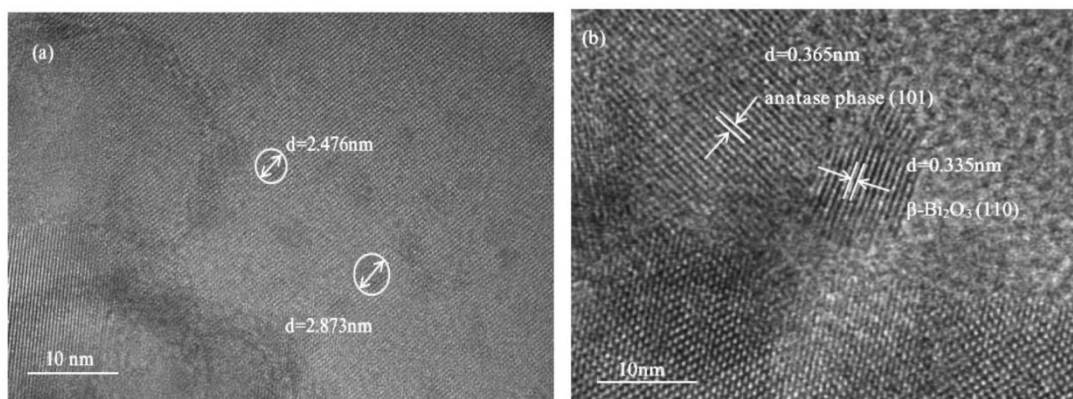


Figure 3. The (a) TEM and (b) HRTEM of 2.1% $\text{Bi}_2\text{O}_3/\text{TiO}_2$.

Table 1. The elemental contents of 2.1% Bi₂O₃/TiO₂ from EDS.

Element	Atomic Fraction (%)	Atomic Error (%)	Mass Fraction (%)	Mass Error (%)	Fit Error (%)
O	61.88	1.29	38.71	0.1	0.61
Ti	37.06	0.38	52.26	0.18	2.57
Bi	1.06	9.03	8.03	9.23	0.19

From the TEM images of Bi₂O₃/TiO₂ composites (Figure 3a), some nanoparticles with a diameter between 2~3 nm are evenly spread on the TiO₂. The HRTEM image of Bi₂O₃/TiO₂ composites (Figure 3b) shows that the lattice fringe is about 0.335 nm, assigned to (110) of β -Bi₂O₃. This indicates that β -Bi₂O₃ is present in the Bi₂O₃/TiO₂ composites. Moreover, the crystal lattice fringe of 0.365 nm is corresponding to the (101) plane of anatase TiO₂. This indicates that the Bi₂O₃ and TiO₂ are closely interlinked. Due the deposition of Bi₂O₃ on TiO₂, it could be profitable to the carriers migrate between Bi₂O₃ and TiO₂ and enhance the separation efficiency of carriers as well as the photocatalytic properties. Furthermore, the crystallite size of Bi₂O₃/TiO₂ composites decreased compared with Bi₂O₃ and TiO₂ [40].

The chemical compositions and element valence state of 2.1%Bi₂O₃/TiO₂ photocatalysts were studied through XPS. Figure 4a displays the XPS survey scan of 2.1%Bi₂O₃/TiO₂, which demonstrates that the presence of Bi, O, and Ti elements can be seen in Bi₂O₃/TiO₂ composites. It indicates that the Bi₂O₃/TiO₂ composites managed to compound by solvothermal method. The high-resolution XPS for Bi 4f of Bi₂O₃/TiO₂ composites is displayed in Figure 4b, and the two main peaks at 159.19 eV and 164.43 eV are corresponding to the Bi 4f_{7/2} and Bi 4f_{5/2}, respectively, which indicates the presence of Bi³⁺ [41]. In addition, the peaks at 157.43 eV and 162.63 eV are attributed to the Bi 0 (metallic Bi) [42], indicating that the Bi³⁺ and metallic Bi are both in Bi₂O₃/TiO₂ composites. Ti 2p peaks of Bi₂O₃/TiO₂ composites are fitted by two XPS peaks (Figure 4c), and the two peaks at 458.19 eV and 463.81 eV are assigned to Ti 2p_{3/2} and Ti 2p_{1/2}, respectively, showing the existence of Ti⁴⁺ [43]. The high-resolution XPS O1s of Bi₂O₃/TiO₂ composites located at 529.36 eV, 530.04 eV, and 531.71 eV belong to lattice oxygen in Bi-O of Bi₂O₃, Ti-O of TiO₂, and surface absorbed hydroxyl groups, respectively (Figure 4d) [44]. It is worth noting that the binding energies of Ti 2p and O1s in 2.1% Bi₂O₃/TiO₂ are shifted towards lower binding energies compared to TiO₂, while Bi 4f binding energy is shifted to high binding energy compared to Bi₂O₃. In conclusion, the XPS results indicate strong interactions and electron transfer between Bi₂O₃ and TiO₂ in Bi₂O₃/TiO₂.

The specific surface areas are important elements to influence the catalytic properties. Therefore, the nitrogen adsorption–desorption isotherm was employed to evaluate the BET surface area of β -Bi₂O₃, TiO₂, and Bi₂O₃/TiO₂ photocatalysts, and the results are shown in Figure 5. The isotherms of all photocatalysts are typical type IV, and the H3 hysteresis loop in the light of IUPAC classification can be observed [45]. It indicates that the β -Bi₂O₃, TiO₂, and Bi₂O₃/TiO₂ photocatalysts are mesoporous structures. The BET specific surface areas of β -Bi₂O₃, TiO₂, and Bi₂O₃/TiO₂ photocatalysts are 3.1, 8.7, and 42.0 m²/g, respectively. Apparently, the specific surface area of Bi₂O₃/TiO₂ composites is considerably increased after the fusion of Bi₂O₃ on TiO₂ compared with pure TiO₂. With the increase of calcination temperature, Bi₅O₇NO₃ gradually transformed to β -Bi₂O₃, and the following decomposition reaction ($\text{Bi}_5\text{O}_7\text{NO}_3 \rightarrow 5/2\text{Bi}_2\text{O}_3 + \text{NO} + 3/4\text{O}_2$) occurs at the calcination temperature. The products of NO and O₂ during the decomposition of Bi₅O₇NO₃ will affect the crystallization process of TiO₂, thus making the TiO₂ structure looser and producing many pores, increasing the specific surface area of the composite. From the SEM results, it can be seen that more holes are formed after the combination of Bi₂O₃ and TiO₂, increasing the specific surface area. In addition, it was reported that the higher specific surface area was frequently accompanied by higher adsorption properties and active sites [46]. Therefore, the Bi₂O₃/TiO₂ composites have a higher adsorption capacity and active sites, indicating the improvement of photocatalytic properties.

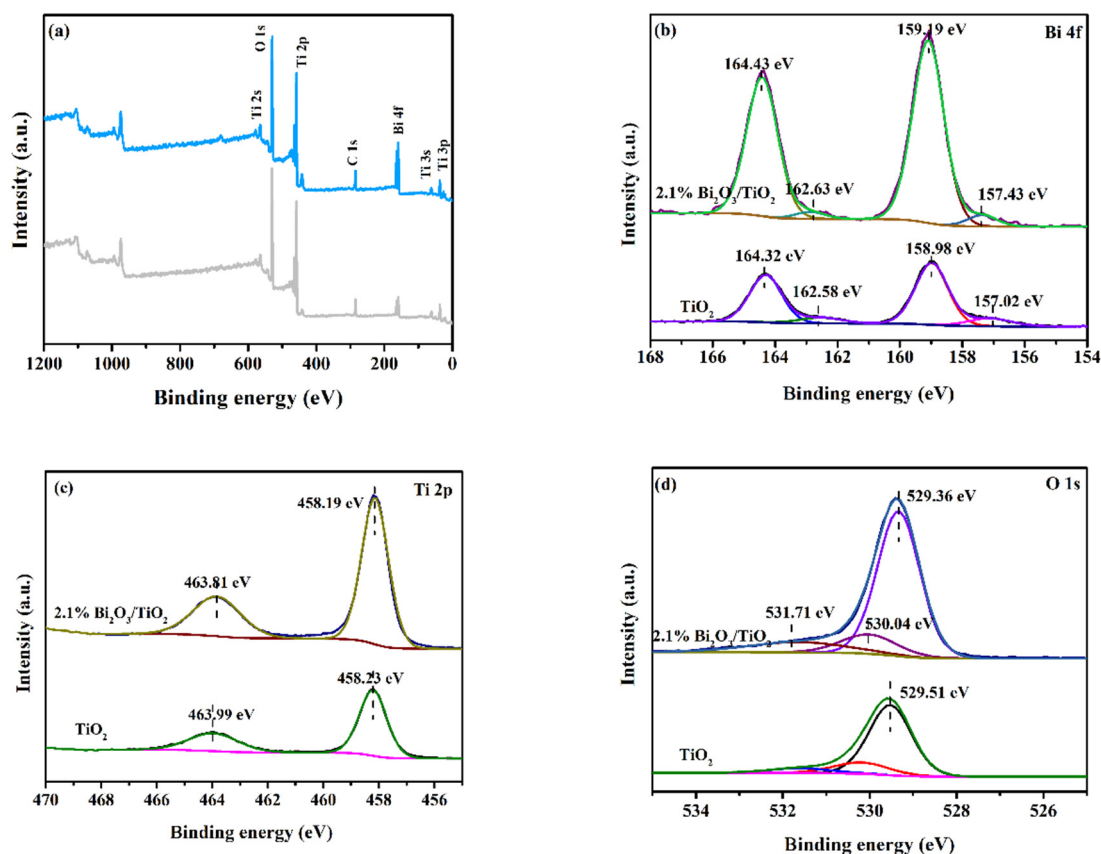


Figure 4. XPS full-spectrum map of 2.1% Bi₂O₃/TiO₂ (a) and high-resolution spectrum map of (b) Bi 4f, (c) Ti 2p, and (d) O 1s.

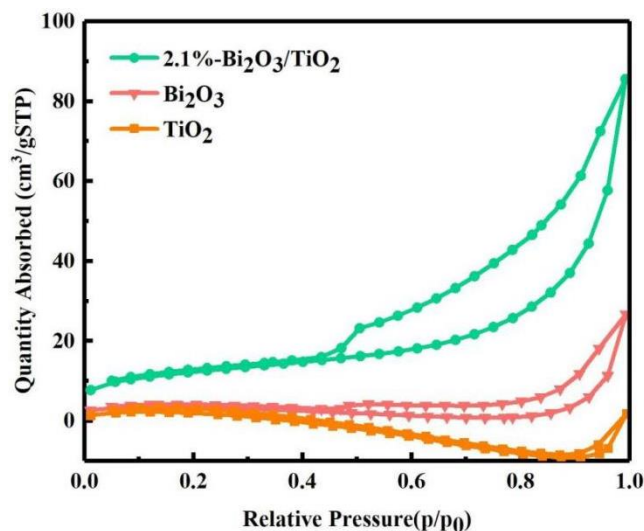


Figure 5. N₂ adsorption–desorption isotherm of 2.1%Bi₂O₃/TiO₂, Bi₂O₃, and TiO₂.

2.2. Analysis of Optical and Photoelectrochemical Performances

The optical properties of pure Bi₂O₃, pure TiO₂, and Bi₂O₃/TiO₂ composites were assessed through UV–vis DRS. As displayed in Figure 6a, obviously, the absorption edge of TiO₂ is about 400 nm in the UV spectrum. However, the Bi₂O₃ has a larger absorption range, and the absorption edge is about 500 nm. For Bi₂O₃/TiO₂ composites, the absorption edges are red-shifted in comparison to the pure TiO₂, particularly 2.1% Bi₂O₃/TiO₂ composites. Therefore, after incorporation of Bi₂O₃, it is profitable to increase the light energy acquirement and visible light absorption for pure TiO₂. It would help to separate

the photogenerated carriers and increase the properties of degradation of RhB. Further, the Kubelka–Munk formula ($\alpha h\nu = A(h\nu - E_g)^{n/2}$) was employed to count the band-gap energy of catalysts [47]. The band gap of pure TiO_2 , pure Bi_2O_3 , and 2.1% $\text{Bi}_2\text{O}_3/\text{TiO}_2$ samples are about 3.1 eV, 2.72 eV, and 2.79 eV, respectively (Figure 6b).

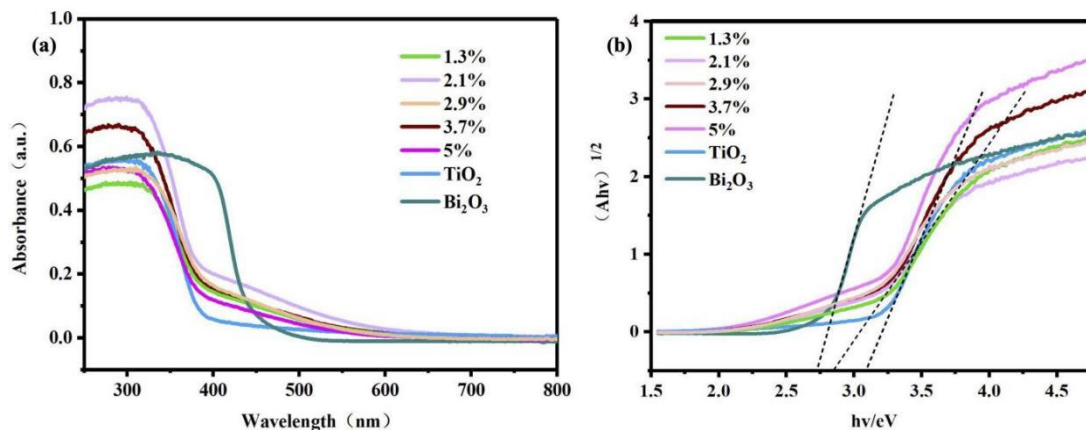


Figure 6. (a) UV-vis spectrum and (b) the band gap of $\text{Bi}_2\text{O}_3/\text{TiO}_2$, Bi_2O_3 , and TiO_2 .

Photoluminescence (PL) was applied to measure the separating efficiency of photogenerated electrons and holes of prepared samples because of its high sensitivity and because it does not destroy contaminated samples. Figure 7 shows the PL results of pure TiO_2 , 1.3% $\text{Bi}_2\text{O}_3/\text{TiO}_2$, 2.1% $\text{Bi}_2\text{O}_3/\text{TiO}_2$, 2.9% $\text{Bi}_2\text{O}_3/\text{TiO}_2$, 3.7% $\text{Bi}_2\text{O}_3/\text{TiO}_2$, and 5% $\text{Bi}_2\text{O}_3/\text{TiO}_2$, respectively. It is evident that the PL intensities of all $\text{Bi}_2\text{O}_3/\text{TiO}_2$ photocatalysts are less than that of pure TiO_2 , implying that the construction of $\text{Bi}_2\text{O}_3/\text{TiO}_2$ restrains the regroup of photogenerated electrons and holes. Meanwhile, the 2.1% $\text{Bi}_2\text{O}_3/\text{TiO}_2$ composite has the lowest intensity, which implies that the separation efficiency of photoinduced carriers is highest, corresponding to the high degradation rate of RhB [45].

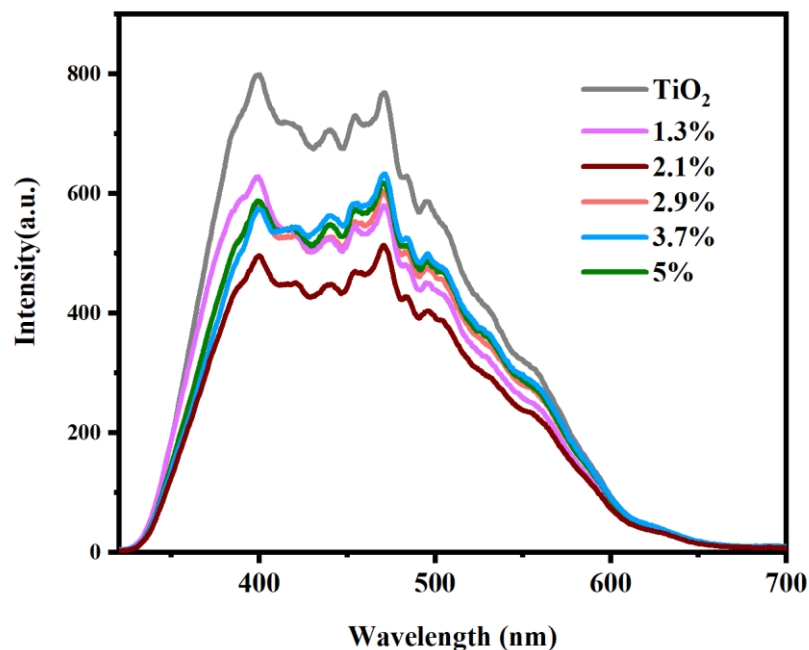


Figure 7. PL fluorescence profiles of TiO_2 and $\text{Bi}_2\text{O}_3/\text{TiO}_2$.

2.3. Photocatalytic Performance Analysis

The photocatalytic properties of pure TiO_2 , pure Bi_2O_3 , and $\text{Bi}_2\text{O}_3/\text{TiO}_2$ composites were assessed by degrading the RhB via simulation sunlight, and the consequences are

displayed in Figure 8. The experiment is divided into two steps: first, in order to achieve concentration balance, the photocatalysts adsorbed the RhB for 30 min under dark reactions; then, the photocatalysts were illuminated under simulated sunlight by xenon lamp. Figure 8a presents the impact of Bi_2O_3 ratio on TiO_2 photocatalytic properties. It is found that the pure Bi_2O_3 , pure TiO_2 , and $\text{Bi}_2\text{O}_3/\text{TiO}_2$ composites have lower absorption ability in the dark after 30 min. However, the photocatalytic performances of $\text{Bi}_2\text{O}_3/\text{TiO}_2$ composites with simulated sunlight increased first with the enhancement of Bi_2O_3 content, and the 2.1% $\text{Bi}_2\text{O}_3/\text{TiO}_2$ composites exhibited exceptional photocatalytic abilities. The degradation rate of RhB can reach 99.6% under the irradiation of simulation sunlight for 60 min, which is about 0.63 of the time and six times better than pure TiO_2 and pure Bi_2O_3 , respectively. It is mainly because of the constitution of the heterojunction between Bi_2O_3 and TiO_2 , which restricts the combination of carriers and thus enhances the photocatalytic properties of the photocatalyst. However, the photocatalytic properties of $\text{Bi}_2\text{O}_3/\text{TiO}_2$ catalysts declined when increasing the Bi_2O_3 content from 2.9% to 5%, which may be the result of the aggregates of the Bi_2O_3 and the drop of active sites. On the other hand, the excessive Bi_2O_3 can be considered as the recombination center, which results in the decrease of photocatalytic properties. The excessive Bi_2O_3 would influence the transmission of light between the Bi_2O_3 and TiO_2 , blocking the motivation of TiO_2 and resulting in reducing the photocatalytic efficiency of photocatalysts [48]. Moreover, the catalytic performances of different $\text{Bi}_2\text{O}_3/\text{TiO}_2$ reported in other papers were compared, and the details are listed in Table 2. It can be seen that the $\beta\text{-Bi}_2\text{O}_3/\text{TiO}_2$ photocatalyst in this work shows the efficient photocatalytic performance for photodegradation RhB.

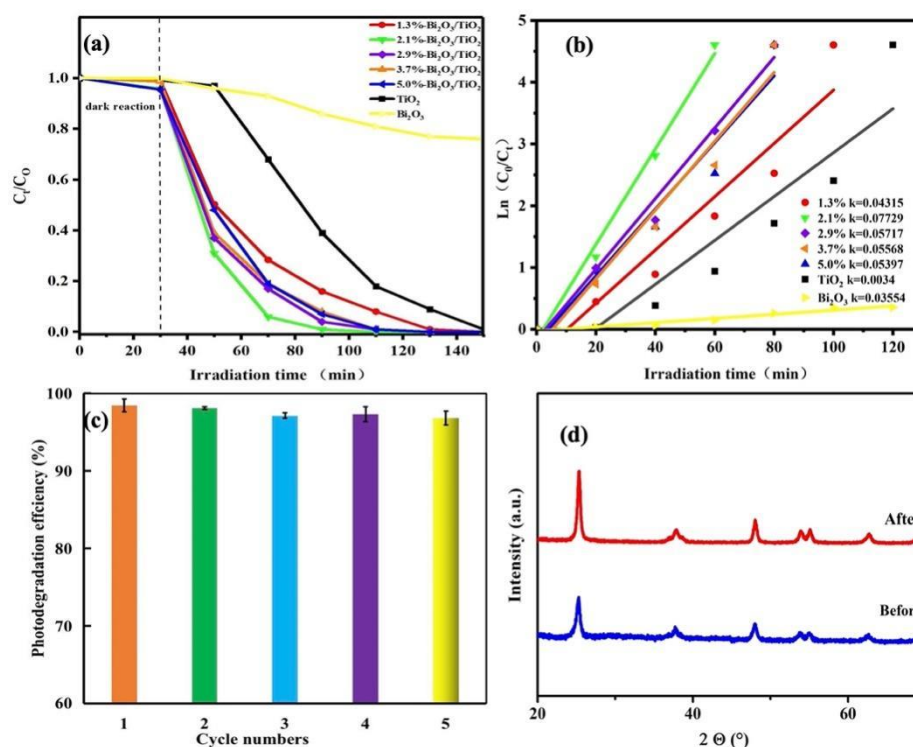


Figure 8. (a) Photocatalytic degradation RhB of catalysts, (b) reaction kinetic constants for degradation, (c) recycle stability of 2.1% $\text{Bi}_2\text{O}_3/\text{TiO}_2$ composites for RhB degradation, and (d) the XRD of before photodegradation and five cycles of photodegradation of 2.1% $\text{Bi}_2\text{O}_3/\text{TiO}_2$ composites.

Table 2. Comparative performance of Bi₂O₃/TiO₂ materials for photocatalytic dye photodegradation.

Catalyst	Degradation Time (min)	Performance (Efficiency (%))	Light Source	Reference
β-Bi ₂ O ₃ /TiO ₂	60 min	100%	Simulated sunlight	this work
Bi ₂ O ₃ /TiO ₂ nanofiber	120 min	65%	Simulated sunlight	[45]
Bi ₂ O ₃ /TiO ₂ -Ph	120 min	87%	Visible light	[35]
Bi ₂ O ₃ /TiO ₂	75 min	99%	Visible light	[49]
TiO ₂ /Bi ₂ O ₃ -g-C ₃ N ₄	120 min	98%	Ultraviolet light/sunlight	[50]
Ag-Bi ₂ O ₃ -TiO ₂	90 min	100%	Full-spectrum light irradiation	[51]

Meanwhile, the first-order reaction rate constant (*k*) determined by quasi-first-order kinetic model was applied to study the photocatalytic processes. As shown in Figure 8b, the *k* values of TiO₂, Bi₂O₃, 1.3%Bi₂O₃/TiO₂, 2.1% Bi₂O₃/TiO₂, 2.9% Bi₂O₃/TiO₂, 3.7% Bi₂O₃/TiO₂, and 5% Bi₂O₃/TiO₂ are 0.03654 h⁻¹, 0.0034 h⁻¹, 0.04315 h⁻¹, 0.07729 h⁻¹, 0.05717 h⁻¹, 0.05568 h⁻¹, and 0.05397 h⁻¹, respectively. It is obvious that the *k* value of 2.1% Bi₂O₃/TiO₂ composites is the maximum, which is 2.1 and 22.7 times of TiO₂ and Bi₂O₃, respectively. The result shows that the 2.1% Bi₂O₃/TiO₂ composites display preferable photocatalytic activity compared to other catalysts. In addition, the recycling stability of the 2.1% Bi₂O₃/TiO₂ composites was assessed. As represented in Figure 8c, the photocatalytic activity of 2.1% Bi₂O₃/TiO₂ composites not to have obvious change after five trials, indicating the outstanding stability and repeatability. Further, in order to verify the stability of 2.1% Bi₂O₃/TiO₂ composites, the XRD was employed to analyze the structure of 2.1% Bi₂O₃/TiO₂ composites before and after five trials, as shown in Figure 8d. It can be seen that there is no obvious change in 2.1% Bi₂O₃/TiO₂ composites before and after five trials, which also implies the stability of Bi₂O₃/TiO₂ composites.

Based on the above analysis, a potential degradation mechanism is put forward. As represented in Figure 9, when the Bi₂O₃/TiO₂ photocatalyst is illuminated by simulated sunlight, the photogenerated electrons (e⁻) are activated and diverted from the CB of TiO₂ to the CB of Bi₂O₃ via the interface of Bi₂O₃/TiO₂ composites; meanwhile, the holes (h⁺) are transferred from the VB of Bi₂O₃ to the VB of TiO₂; therefore, the photoinduced holes accumulate in the heterojunction interface, which is favorable for the separation of photogenerated electrons and holes. The photogenerated electron and holes could have the following reactions [52]: On the one hand, the electrons react with O₂ in the solution to produce •O₂⁻. Then, the H⁺ react with the •O₂⁻ to generate H₂O₂, which then reacts with electrons to transform •OH. On the other hand, the h⁺ on the VB of TiO₂ oxidizes the H₂O/OH⁻ to form •OH radicals for RhB degradation. Therefore, the Bi₂O₃/TiO₂ composites have higher photocatalytic activity.

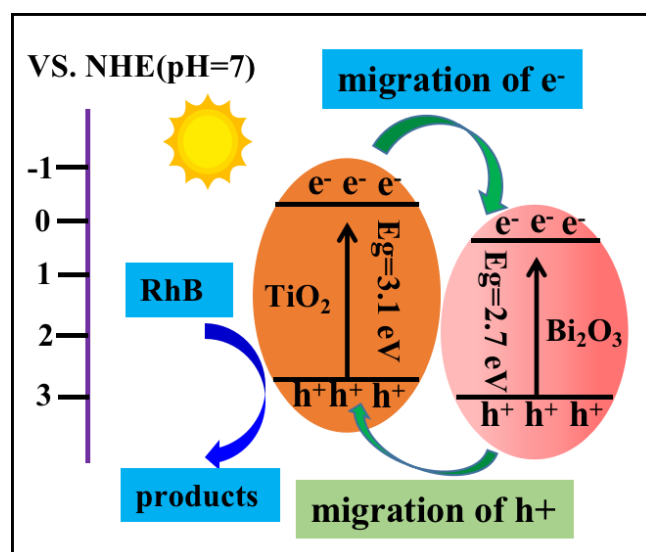


Figure 9. Photocatalytic mechanism based on degradation of the RhB of the $\text{Bi}_2\text{O}_3/\text{TiO}_2$ photocatalyst.

3. Experimental

3.1. Chemicals

Titanium tetrachloride was purchased from Shanghai Nuotai Chemical Co., Ltd, Shanghai, China. Sinopharm Chemical Reagent Co., Ltd, Shanghai, China. provided nitric acid (HNO_3 , AR), bismuth nitrate pentahydrate ($\text{Bi}(\text{NO}_3)_3 \cdot 5\text{H}_2\text{O}$, AR), and sodium bicarbonate (NaHCO_3 , AR). Sodium hydroxide (NaOH , AR) and glycerol were obtained from Xilong Chemical Co., Ltd, Guangzhou, China. Ethanol ($\text{CH}_3\text{CH}_2\text{O}$, AR) was obtained from Aladdin. Rhodamine B was provided by Shanghai Yuanye Biotechnology Co., Ltd, Shanghai, China.

3.2. Preparation of $\beta\text{-Bi}_2\text{O}_3/\text{TiO}_2$ Photocatalysts

$\text{Bi}(\text{NO}_3)_3 \cdot 5\text{H}_2\text{O}$, 30 mL glycerin, and 20 mL ethanol were mixed together and then stirred for 30 min and sonicated for 1 min. The mixtures were poured into a Teflon-sealed reactor. Titanium tetrachloride was added drop by drop into the solution. Then, the Teflon-sealed reactor was put into an oven and heated for 48 h at 110 °C. When the temperature dropped to 25 °C, the reaction productions were collected and washed with ethanol several times and dried at 80 °C for 6 h to obtain the material. The material was calcined at 375 °C for 4 h to obtain the product. The molar ratios of Bi/Ti in the composites were settled at 1.3%, 2.1%, 2.9%, 3.7%, and 5.0%, which were calculated by theoretical methods. The as-prepared photocatalysts were denoted as 1.3%, 2.1%, 2.9%, 3.7%, and 5.0% $\text{Bi}_2\text{O}_3/\text{TiO}_2$, which are based on the molar ratio of Bi/Ti. As a comparison, pure Bi_2O_3 and TiO_2 samples were prepared with the same procedure.

3.3. Characterization

The crystal structure was studied by a X-ray diffraction (XRD, Rigaku, RINT2000 with $\text{Cu K } \alpha$ radiation ($\lambda = 0.15418$ nm)). The morphologies of photocatalysts were studied through a field-induced emission scanning electron microscope (FESEM, JSM-6700F). The transmission electron microscopy (TEM) was employed by JEM-2010F, and the accelerating voltage was 200 kV. The Brunauer–Emmett–Teller (BET) specific surface area of prepared photocatalysts was recorded on a Quantachrome NOVA 2000e. A UV–vis scanning spectrophotometer (UV–vis/DRS, SHIMADZU UV-2450) was applied to investigate the optical properties of the prepared photocatalysts. The photoluminescence (PL) was measured by a Hitachi F4500 fluorescence spectrometer. The X-ray photoelectron spectroscopy (XPS, ESCALAB MK II) was employed to analyze the elemental compositions of the samples.

3.4. Photocatalytic Activity Analysis

The photocatalytic properties of all photocatalysts were analyzed by degrading rhodamine B (RhB) with simulation sunlight illumination. The illuminant was a 300 W Xe lamp (PLS-SXE300, Beijing Park Lay Technology Co., Ltd., Beijing, China), and the light intensity was 100 mW/cm². Briefly, the photocatalyst (50 mg) was placed into 60 mL of 20 mg/L of RhB solution. Before exposure to light, the mixture solution was stirred for 30 min to obtain adsorption equilibrium. Then, 3 mL of solution was extracted and centrifuged at 20 min intervals. The RhB concentration was recorded through the UV–vis spectrophotometer. The stability of Bi₂O₃/TiO₂ photocatalyst was studied via five recycling experiments, and the results were the average value of three samples.

4. Conclusions

In this study, flower-like Bi₂O₃/TiO₂ photocatalysts were successfully prepared by solvothermal route, and XRD, SEM, TEM, XPS, BET, UV–vis, and PL were employed to analyze the morphology and properties of the photocatalysts. The influence of doped Bi₂O₃ content on TiO₂ photocatalytic efficiency was determined. The XRD results implied that the presence of Bi₂O₃ did not destroy the lattice structure of TiO₂. The photocatalytic properties of materials were studied via RhB degradation. A significantly improvement in photoactivity was obtained when the heterojunction was created between Bi₂O₃ and TiO₂. Further, the 2.1% Bi₂O₃/TiO₂ photocatalyst has the best degradation efficiency, which is 99.6% degradation of RhB at 60 min. It is mainly because the heterojunction in Bi₂O₃/TiO₂ strengthens the movement and separation of carriers and then enhances the photocatalytic properties of the Bi₂O₃/TiO₂.

Author Contributions: Experiments, M.W. and C.L.; Analysed, B.L. and W.Q.; Writing, M.W., C.L. and B.L.; Revised, W.Q.; Funding, Y.X. and M.W. All authors have read and agreed to the published version of the manuscript.

Funding: This work was financially supported by the Science and Technology Department of Jiangxi Province (20181ACG70025) and the Key Project of Science and Technology Research of Jiangxi Provincial Department of Education (No. GJJ191044). This work was also supported by Shanghai Summit Discipline in Design (SJGFJK-2019-001), Jiangxi Province “double thousand plan” project (jxsq2019201007), and Jiangxi Province’s Scientific Planning Project (No. YG2021057).

Institutional Review Board Statement: Not applicable.

Informed Consent Statement: Not applicable.

Data Availability Statement: Data of the present study are available in the article.

Conflicts of Interest: The authors declare no conflict of interest.

Sample Availability: Samples of the compounds are available from the authors.

References

1. Mukhtar, F.; Munawar, T.; Nadeem, M.S.; Khan, S.A.; Koc, M.; Batool, S.; Hasan, M.; Iqbal, F. Enhanced sunlight-absorption of Fe₂O₃ covered by PANI for the photodegradation of organic pollutants and antimicrobial inactivation. *Adv. Powder Technol.* **2022**, *33*, 103708. [[CrossRef](#)]
2. Luo, J.; Dai, Z.; Feng, M.; Gu, M.; Xie, Y. Graphitic carbon nitride/ferroferric oxide/reduced graphene oxide nanocomposite as highly active visible light photocatalyst. *Nano Res.* **2022**, *16*, 371–376. [[CrossRef](#)]
3. Cui, H.; Zhou, Y.; Mei, J.; Li, Z.; Xu, S.; Yao, C. Synthesis of CdS/BiOBr nanosheets composites with efficient visible-light photocatalytic activity. *J. Phys. Chem. Solids* **2018**, *112*, 80–87. [[CrossRef](#)]
4. Weng, B.; Lu, K.-Q.; Tang, Z.; Chen, H.M.; Xu, Y.-J. Stabilizing ultrasmall Au clusters for enhanced photoredox catalysis. *Nat. Commun.* **2018**, *9*, 1543. [[CrossRef](#)] [[PubMed](#)]
5. Huang, H.; Verhaeghe, D.; Weng, B.; Ghosh, B.; Zhang, H.; Hofkens, J.; Steele, J.A.; Roeffaers, M.B.J. Metal Halide Perovskite-Based Heterojunction Photocatalysts. *Angew. Chem. Int. Ed.* **2022**, *134*, e202203261.
6. Liao, H.; Liu, C.; Zhong, J.; Li, J. Fabrication of BiOCl with adjustable oxygen vacancies and greatly elevated photocatalytic activity by using bamboo fiber surface embellishment. *Colloids Surf. A Physicochem. Eng. Asp.* **2022**, *634*, 127892. [[CrossRef](#)]

7. Jiang, L.; Guo, Y.; Pan, J.; Zhao, J.; Ling, Y.; Xie, Y.; Zhou, Y.; Zhao, J. N. P, O co-doped carbon filling into carbon nitride microtubes to promote photocatalytic hydrogen production. *Sci. Total Environ.* **2022**, *809*, 151114. [[CrossRef](#)]
8. Huang, H.; Zhao, J.; Weng, B.; Lai, F.; Zhang, M.; Hofkens, J.; Roeyfaers, M.B.J.; Steele, J.A.; Long, J. Site-Sensitive Selective CO₂ Photoreduction to CO over Gold Nanoparticles. *Angew. Chem. Int. Ed.* **2022**, *134*, e202204563.
9. Wu, W.; Sun, Y.; Zhou, H. In-situ construction of β -Bi₂O₃/Ag₂O photocatalyst from deactivated AgBiO₃ for tetracycline degradation under visible light. *Chem. Eng. J.* **2022**, *432*, 134316. [[CrossRef](#)]
10. Shen, Z.; Zhou, Y.; Guo, Y.; Zhao, J.; Song, J.; Xie, Y.; Ling, Y.; Zhang, W. Tuning the concentration of surface/bulk oxygen vacancies in CeO₂ nanorods to promote highly efficient photodegradation of organic dyes. *Chin. Chem. Lett.* **2021**, *32*, 2524–2528. [[CrossRef](#)]
11. Mukhtar, F.; Munawar, T.; Nadeem, M.S.; ur Rehman, M.N.; Mahmood, K.; Batool, S.; Hasan, M.; ur Rehman, K.; Iqbal, F. Enhancement in carrier separation of ZnO-Ho₂O₃-Sm₂O₃ heterostructured nanocomposite with rGO and PANI supported direct dual Z-scheme for antimicrobial inactivation and sunlight driven photocatalysis. *Adv. Powder Technol.* **2021**, *32*, 3770–3787. [[CrossRef](#)]
12. Mukhtar, F.; Munawar, T.; Nadeem, M.S.; ur Rehman, M.N.; Batool, S.; Hasan, M.; Riaz, M.; ur Rehman, K.; Iqbal, F. Highly efficient tri-phase TiO₂-Y₂O₃-V₂O₅ nanocomposite: Structural, optical, photocatalyst, and antibacterial studies. *J. Nanostruct. Chem.* **2022**, *12*, 547–564. [[CrossRef](#)]
13. Qutub, N.; Singh, P.; Sabir, S.; Sagadevan, S.; Oh, W.C. Enhanced photocatalytic degradation of Acid Blue dye using CdS/TiO₂ nanocomposite. *Sci. Rep.* **2022**, *12*, 5759. [[CrossRef](#)] [[PubMed](#)]
14. Chen, L.; Song, X.-L.; Ren, J.-T.; Yuan, Z.-Y. Precisely modifying Co₂P/black TiO₂ S-scheme heterojunction by in situ formed P and C dopants for enhanced photocatalytic H₂ production. *Appl. Catal. B Environ.* **2022**, *315*, 121546. [[CrossRef](#)]
15. Nemiwal, M.; Zhang, T.C.; Kumar, D. Recent progress in g-C₃N₄, TiO₂ and ZnO based photocatalysts for dye degradation: Strategies to improve photocatalytic activity. *Sci. Total Environ.* **2021**, *767*, 144896. [[CrossRef](#)]
16. Zhu, G.; Feng, S.; Chao, J.; Zheng, W.; Shao, C. One-pot synthesis of C-dots modified TiO₂ nanosheets/UiO-66-NH₂ with improved photocatalytic activity under visible light. *Ceram. Int.* **2020**, *46*, 2530–2537. [[CrossRef](#)]
17. Li, Z.; Wang, S.; Wu, J.; Zhou, W. Recent progress in defective TiO₂ photocatalysts for energy and environmental applications. *Renew. Sustain. Energy Rev.* **2022**, *156*, 111980. [[CrossRef](#)]
18. Jin, Y.; Tang, W.; Wang, J.; Ren, F.; Chen, Z.; Sun, Z.; Ren, P.-G. Construction of biomass derived carbon quantum dots modified TiO₂ photocatalysts with superior photocatalytic activity for methylene blue degradation. *J. Alloys Compd.* **2023**, *932*, 167627. [[CrossRef](#)]
19. Tashkandi, N.Y.; Albukhari, S.M.; Ismail, A.A. Visible-light driven of heterostructured LaFeO₃/TiO₂ photocatalysts for degradation of antibiotics: Ciprofloxacin as case study. *J. Photochem. Photobiol. A Chem.* **2022**, *432*, 114078. [[CrossRef](#)]
20. Wang, H.; Song, L.; Yu, L.; Xia, X.; Bao, Y.; Lourenco, M.; Homewood, K.; Gao, Y. Charge transfer between Ti⁴⁺, Sn⁴⁺ and Pt in the tin doped TiO₂ photocatalyst for elevating the hydrogen production efficiency. *Appl. Surf. Sci.* **2022**, *581*, 152202. [[CrossRef](#)]
21. Basavarajappa, P.S.; Patil, S.B.; Ganganagappa, N.; Reddy, K.R.; Raghu, A.V.; Reddy, C.V. Recent progress in metal-doped TiO₂, non-metal doped/codoped TiO₂ and TiO₂ nanostructured hybrids for enhanced photocatalysis. *Int. J. Hydrogen Energy* **2020**, *45*, 7764–7778. [[CrossRef](#)]
22. Zhang, C.; Zhou, Y.; Bao, J.; Fang, J.; Zhao, S.; Zhang, Y.; Sheng, X.; Chen, W. Structure regulation of ZnS@g-C₃N₄/TiO₂ nanospheres for efficient photocatalytic H₂ production under visible-light irradiation. *Chem. Eng. J.* **2018**, *346*, 226–237. [[CrossRef](#)]
23. Niu, M.; Cao, D.; Sui, K.; Liu, C. InP/TiO₂ heterojunction for photoelectrochemical water splitting under visible-light. *Int. J. Hydrogen Energy* **2020**, *45*, 11615–11624. [[CrossRef](#)]
24. Meng, A.; Cheng, B.; Tan, H.; Fan, J.; Su, C.; Yu, J. TiO₂/polydopamine S-scheme heterojunction photocatalyst with enhanced CO₂-reduction selectivity. *Appl. Catal. B Environ.* **2021**, *289*, 120039. [[CrossRef](#)]
25. Zeng, D.; Wang, J.; Xie, Y.; Ling, Y.; Zhao, J.; Ye, H.; Chen, T. TiO₂@ZnFe₂O₄ heterojunctions for efficient photocatalytic degradation of persistent pollutants and hydrogen evolution. *Mater. Chem. Phys.* **2022**, *277*, 125462. [[CrossRef](#)]
26. Ge, H.; Xu, F.; Cheng, B.; Yu, J.; Ho, W. S-Scheme heterojunction TiO₂/CdS nanocomposite nanofiber as H₂-production photocatalyst. *ChemCatChem* **2019**, *11*, 6301–6309. [[CrossRef](#)]
27. Wang, J.; Wang, G.; Cheng, B.; Yu, J.; Fan, J. Sulfur-doped g-C₃N₄/TiO₂ S-scheme heterojunction photocatalyst for Congo Red photodegradation. *Chin. J. Catal.* **2021**, *42*, 56–68. [[CrossRef](#)]
28. Zhang, X.; Shi, Q.; Liu, X.; Li, J.; Xu, H.; Ding, H.; Li, G. Facile Assembly of InVO₄/TiO₂ Heterojunction for Enhanced Photo-Oxidation of Benzyl Alcohol. *Nanomaterials* **2022**, *12*, 1544. [[CrossRef](#)]
29. Lu, H.; Hao, Q.; Chen, T.; Zhang, L.; Chen, D.; Ma, C.; Yao, W.; Zhu, Y. A high-performance Bi₂O₃/Bi₂SiO₅ p-n heterojunction photocatalyst induced by phase transition of Bi₂O₃. *Appl. Catal. B Environ.* **2018**, *237*, 59–67. [[CrossRef](#)]
30. Bao, Y.; Lim, T.-T.; Zhong, Z.; Wang, R.; Hu, X. Acetic acid-assisted fabrication of hierarchical flower-like Bi₂O₃ for photocatalytic degradation of sulfamethoxazole and rhodamine B under solar irradiation. *J. Colloid Interface Sci.* **2017**, *505*, 489–499. [[CrossRef](#)]
31. Jiang, T.; Cheng, L.; Han, Y.; Feng, J.; Zhang, J. One-pot hydrothermal synthesis of Bi₂O₃-WO₃ p-n heterojunction film for photoelectrocatalytic degradation of norfloxacin. *Sep. Purif. Technol.* **2020**, *238*, 116428. [[CrossRef](#)]
32. Tang, X.; Ma, C.; Liu, N.; Liu, C.; Liu, S. Visible light β -Bi₂O₃/BiOCl heterojunction photocatalyst with highly T enhanced photocatalytic activity. *Chem. Phys. Lett.* **2018**, *709*, 82–87. [[CrossRef](#)]

33. Majumder, S.; Quang, N.D.; Hien, T.T.; Chinh, N.D.; Yang, H.; Kim, C.; Kim, D. Nanostructured β -Bi₂O₃/PbS heterojunction as np-junction photoanode for enhanced photoelectrochemical performance. *J. Alloys Compd.* **2021**, *870*, 159545. [[CrossRef](#)]
34. Liu, X.; Kang, Y.; Wang, Y. Novel high-efficiency visible-light-driven p-n heterojunction beta-Bi₂O₃/Ag₂WO₄ photocatalysts. *Chem. Phys. Lett.* **2022**, *790*, 139347. [[CrossRef](#)]
35. Lou, B.; Chen, C.; Liu, J.; Zou, S.; Xiao, L.; Fan, J. Selectively depositing Bi₂O₃ quantum dots on TiO₂ nanotubes for efficient visible-light-driven photocatalysis. *Mater. Lett.* **2021**, *288*, 129413. [[CrossRef](#)]
36. Reddy, N.L.; Emin, S.; Valant, M.; Shankar, M.V. Nanostructured Bi₂O₃@TiO₂ photocatalyst for enhanced hydrogen production. *Int. J. Hydrogen Energy* **2017**, *42*, 6627–6636. [[CrossRef](#)]
37. Wei, K.; Armutlulu, A.; Wang, Y.; Yao, G.; Xie, R.; Lai, B. Visible-light-driven removal of atrazine by durable hollow core-shell TiO₂@LaFeO₃ heterojunction coupling with peroxymonosulfate via enhanced electron-transfer. *Appl. Catal. B Environ.* **2022**, *303*, 120889. [[CrossRef](#)]
38. Shamaila, S.; Sajjad, A.K.L.; Chen, F.; Zhang, J. Study on highly visible light active Bi₂O₃ loaded ordered mesoporous titania. *Appl. Catal. B Environ.* **2010**, *94*, 272–280. [[CrossRef](#)]
39. Zhu, J.; Wang, S.; Wang, J.; Zhang, D.; Li, H. Highly active and durable Bi₂O₃/TiO₂ visible photocatalyst in flower-like spheres with surface-enriched Bi₂O₃ quantum dots. *Appl. Catal. B Environ.* **2011**, *102*, 120–125. [[CrossRef](#)]
40. Mukhtar, F.; Munawar, T.; Nadeem, M.S.; ur Rehman, M.N.; Khan, S.A.; Koc, M.; Batool, S.; Hasan, C.M.; Iqbal, F. Dual Z-scheme core-shell PANI-CeO₂-Fe₂O₃-NiO heterostructured nanocomposite for dyes remediation under sunlight and bacterial disinfection. *Environ. Res.* **2022**, *215*, 114140. [[CrossRef](#)]
41. Chen, J.; Tang, T.; Feng, W.; Liu, X.; Yin, Z.; Zhang, X.; Chen, J.; Cao, S. Large-Scale synthesis of p–n Heterojunction Bi₂O₃/TiO₂ nanostructures as photocatalysts for removal of antibiotics under visible light. *ACS Appl. Nano Mater.* **2022**, *5*, 1296–1307. [[CrossRef](#)]
42. Xu, D.; Hai, Y.; Zhang, X.; Zhang, S.; He, R. Bi₂O₃ cocatalyst improving photocatalytic hydrogen evolution performance of TiO₂. *Appl. Surf. Sci.* **2017**, *400*, 530–536. [[CrossRef](#)]
43. Hu, J.; Zhao, R.; Li, H.; Xu, Z.; Dai, H.; Gao, H.; Yu, H.; Wang, Z.; Wang, Y.; Liu, Y.; et al. Boosting visible light photocatalysis in an Au@TiO₂ yolk-in-shell nanohybrid. *Appl. Catal. B Environ.* **2022**, *303*, 120869. [[CrossRef](#)]
44. Alhaddad, M.; Ismail, A.A.; Alghamdi, Y.G.; Al-Khathami, N.D.; Mohamed, R.M. Co₃O₄ Nanoparticles Accommodated Mesoporous TiO₂ framework as an Excellent Photocatalyst with Enhanced Photocatalytic Properties. *Opt. Mater.* **2022**, *131*, 112643. [[CrossRef](#)]
45. He, R.; Liu, H.; Liu, H.; Xu, D.; Zhang, L. S-scheme photocatalyst Bi₂O₃/TiO₂ nanofiber with improved photocatalytic performance. *J. Mater. Sci. Technol.* **2020**, *52*, 145–151.
46. Huang, Y.; Zhang, J.; Dai, K.; Liang, C.; Dawson, G. Efficient solar-driven CO₂ reduction on aminated 2D/2D BiOBr/CdS-diethylenetriamine S-scheme heterojunction. *Ceram. Int.* **2022**, *48*, 8423–8432. [[CrossRef](#)]
47. Wang, T.; Xiao, G.; Li, C.; Zhong, S.; Zhang, F. One-step synthesis of a sulfur doped Bi₂WO₆/Bi₂O₃ composite with enhanced visible-light photocatalytic activity. *Mater. Lett.* **2015**, *138*, 81–84. [[CrossRef](#)]
48. Zhu, P.; Xu, J.; Xie, L.; Duan, M.; Wu, X.; Xiao, X.; Liu, M. Preparation and characterization of highly efficient Z-scheme oxygen vacancy-BiOBr/CoFe₂O₄ heterojunction photocatalyst driven by visible light for antibiotic degradation. *Colloids Surf. A Physicochem. Eng. Asp.* **2022**, *645*, 128810. [[CrossRef](#)]
49. Huang, Y.; Weib, Y.; Wang, J.; Luo, D.; Fan, L.; Wu, J. Controllable fabrication of Bi₂O₃/TiO₂ heterojunction with excellent visible-light responsive photocatalytic performance. *Appl. Surf. Sci.* **2017**, *423*, 119–130. [[CrossRef](#)]
50. Jing, H.; Gao, Y.; Li, L.; Wang, X.; Pei, W.; Yang, X. Synthesis of a Novel Double Z-Scheme TiO₂/Bi₂O₃-g-C₃N₄ Photocatalyst with Enhanced Photocatalytic Performance to Rhodamine B Under Sunlight. *J. Clust. Sci.* **2022**, *1–8*. [[CrossRef](#)]
51. Wang, Y.; Zhao, S.; Yang, Y.; Rodriguez, R.D.; Lipovka, A.; Lu, Y.; Huang, H.; Chen, J. Ag nanoparticle-decorated Bi₂O₃-TiO₂ heterogeneous nanotubular photocatalysts for enhanced degradation of organic contaminants. *Colloids Surf. A Physicochem. Eng. Asp.* **2022**, *648*, 129233. [[CrossRef](#)]
52. Gurugubelli, T.R.; Ravikumar, R.V.; Koutavarapu, R. Enhanced photocatalytic activity of ZnO–CdS composite nanostructures towards the degradation of Rhodamine B under solar Light. *Catalysts* **2022**, *12*, 84. [[CrossRef](#)]

Disclaimer/Publisher’s Note: The statements, opinions and data contained in all publications are solely those of the individual author(s) and contributor(s) and not of MDPI and/or the editor(s). MDPI and/or the editor(s) disclaim responsibility for any injury to people or property resulting from any ideas, methods, instructions or products referred to in the content.